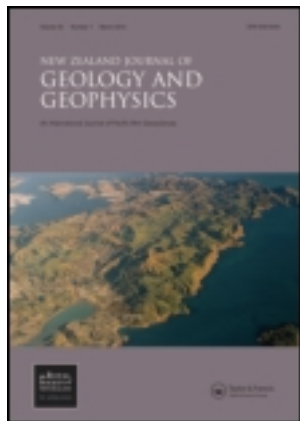


This article was downloaded by: [University of California, Berkeley]

On: 08 November 2011, At: 09:38

Publisher: Taylor & Francis

Informa Ltd Registered in England and Wales Registered Number: 1072954 Registered office: Mortimer House, 37-41 Mortimer Street, London W1T 3JH, UK



New Zealand Journal of Geology and Geophysics

Publication details, including instructions for authors and subscription information:
<http://www.tandfonline.com/loi/tnzg20>

Palaeoseismic constraints on Holocene surface ruptures along the Ostler Fault, southern New Zealand

CB Amos^a, JJ Lapwood^b, DC Nobes^b, DW Burbank^c, U Rieser^d & A Wade^e

^a Department of Earth & Planetary Science, University of California, Berkeley, CA, USA

^b Department of Geological Sciences, University of Canterbury, Christchurch, NZ

^c Department of Earth Science, University of California, Santa Barbara, CA, USA

^d School of Geography, Environment and Earth Sciences, Victoria University of Wellington, Wellington, NZ

^e Fugro Consultants, Inc., Walnut Creek, CA, US

Available online: 07 Nov 2011

To cite this article: CB Amos, JJ Lapwood, DC Nobes, DW Burbank, U Rieser & A Wade (2011): Palaeoseismic constraints on Holocene surface ruptures along the Ostler Fault, southern New Zealand, *New Zealand Journal of Geology and Geophysics*, 54:4, 367-378

To link to this article: <http://dx.doi.org/10.1080/00288306.2011.601746>

PLEASE SCROLL DOWN FOR ARTICLE

Full terms and conditions of use: <http://www.tandfonline.com/page/terms-and-conditions>

This article may be used for research, teaching, and private study purposes. Any substantial or systematic reproduction, redistribution, reselling, loan, sub-licensing, systematic supply, or distribution in any form to anyone is expressly forbidden.

The publisher does not give any warranty express or implied or make any representation that the contents will be complete or accurate or up to date. The accuracy of any instructions, formulae, and drug doses should be independently verified with primary sources. The publisher shall not be liable for any loss, actions, claims, proceedings, demand, or costs or damages whatsoever or howsoever caused arising directly or indirectly in connection with or arising out of the use of this material.

Palaeoseismic constraints on Holocene surface ruptures along the Ostler Fault, southern New Zealand

CB Amos^{a*}, JJ Lapwood^{b†}, DC Nobes^b, DW Burbank^c, U Rieser^d and A Wade^e

^aDepartment of Earth & Planetary Science, University of California, Berkeley, CA, USA; ^bDepartment of Geological Sciences, University of Canterbury, Christchurch, NZ; ^cDepartment of Earth Science, University of California, Santa Barbara, CA, USA; ^dSchool of Geography, Environment and Earth Sciences, Victoria University of Wellington, Wellington, NZ; ^eFugro Consultants, Inc., Walnut Creek, CA, US

Palaeoseismic trenching along the central Ostler fault zone reveals the nature and timing of past surface-rupturing earthquakes. A 26 m long trench excavated into a last-glacial (26.5 ka) outwash surface cut by the Ruataniwha strand of the North Central Ostler fault reveals evidence for at least two metre-scale surface displacements in the last c. 8 ka. Detailed logging of colluvial wedge and alluvial stratigraphy, combined with optically stimulated luminescence dating of loess within colluvial packages, provides a maximum bound on the most recent earthquake (MRE) of 2.3–4.5 ka. The MRE resulted in a surface displacement of at least 1.8 m, consistent with an estimated moment magnitude (M) 6.9–7.1 earthquake based on the total 60 km length of the Ostler fault zone. The penultimate event occurred sometime before 4.1–8.4 ka and resulted in a comparable or larger surface displacement. Similar ages from samples collected in previous trenches on the Ostler fault suggest that surface ruptures may persist across kilometre-scale stepovers defined by the active surface trace of the fault. At the trench scale, comparison between dip slip calculated from topographic fault-scarp profiling (7.8 m) and the total offset of exposed outwash gravels (6.0 m) suggests that surface folding immediately adjacent to the fault scarp accommodates roughly 25% of the total slip. Given a previously reported recurrence interval of c. 2–5 ka for the Ostler fault, the presence of only 2–3 palaeoearthquakes on the 26.5 ka outwash surface indicates that additional events likely occurred on nearby fault scarps in an overall complex zone of surface faulting.

Keywords: earthquake recurrence; luminescence dating; neotectonics; Ostler fault; palaeoseismicity; seismic hazard; Southern Alps

Introduction

The Ostler fault is a zone of east-directed reverse faulting within the intermontane Mackenzie Basin in the Southern Alps of New Zealand (Fig. 1). The fault represents one of several structures east of the plate-bounding Alpine fault that accommodate approximately one-quarter to one-third of the 37 mm a⁻¹ of relative motion between the obliquely colliding Pacific and Australian plates (DeMets et al. 1994; Pearson et al. 1995; Norris & Cooper 2001). Previous work on the structural and geomorphic evolution of the Ostler fault suggests a rate of late-Quaternary slip of c. 1–2 mm a⁻¹ from deformed geomorphic surfaces (Blick et al. 1989; Read & Blick 1991; Amos et al. 2007; Amos et al. 2010) and seismic reflection profiling (Ghisetti et al. 2007). Curiously, repeated level-line surveying related to construction of the Ohau-A Power Project near Twizel (Fig. 1) documents ongoing vertical deformation and anticlinal warping of the fault's hanging wall comparable to the overall fault slip rate (Blick et al. 1989). This observation raises the question whether the Ostler fault zone slips coseismically during large surface-rupturing earthquakes, or whether a component of the permanent deformation across the fault represents the product of aseismic creep. Fault trenching on the Northern fault section (Fig. 1) confirms the presence of several

coseismic ruptures during the Holocene by documenting colluvial wedge deposits adjacent to and deformed across the fault scarp (van Dissen et al. 1994). The question remains, however, whether these earthquakes also ruptured central portions of the Ostler fault, where aseismic folding may accommodate some component of the total deformation.

New palaeoseismic trenching provides constraints on the history of past earthquakes along the Ruataniwha strand of the North Central Ostler fault, immediately west of Twizel (Figs. 1 and 2). Here we present detailed logging of exposed trench stratigraphy and the results of optically stimulated luminescence (OSL) dating of colluvial wedges to characterise the size, timing and frequency of ancient surface-rupturing earthquakes. This work confirms the presence of multiple metre-scale coseismic displacements during the Holocene in the vicinity of the original levelling surveys (Blick et al. 1989). Comparison with documented palaeoearthquakes on the northern Ostler fault zone also enables assessment of kilometre-scale stepovers in the surface trace of the fault (Fig. 1) as potential barriers to rupture propagation. Additionally, this work allows evaluation of the relative contribution of coseismic displacement versus hanging-wall folding to the total deformation over an individual fault scarp.

*Corresponding author. Email: cbamos@seismo.berkeley.edu

†Present address: Rio Tinto Iron Ore, Perth, WA, Australia

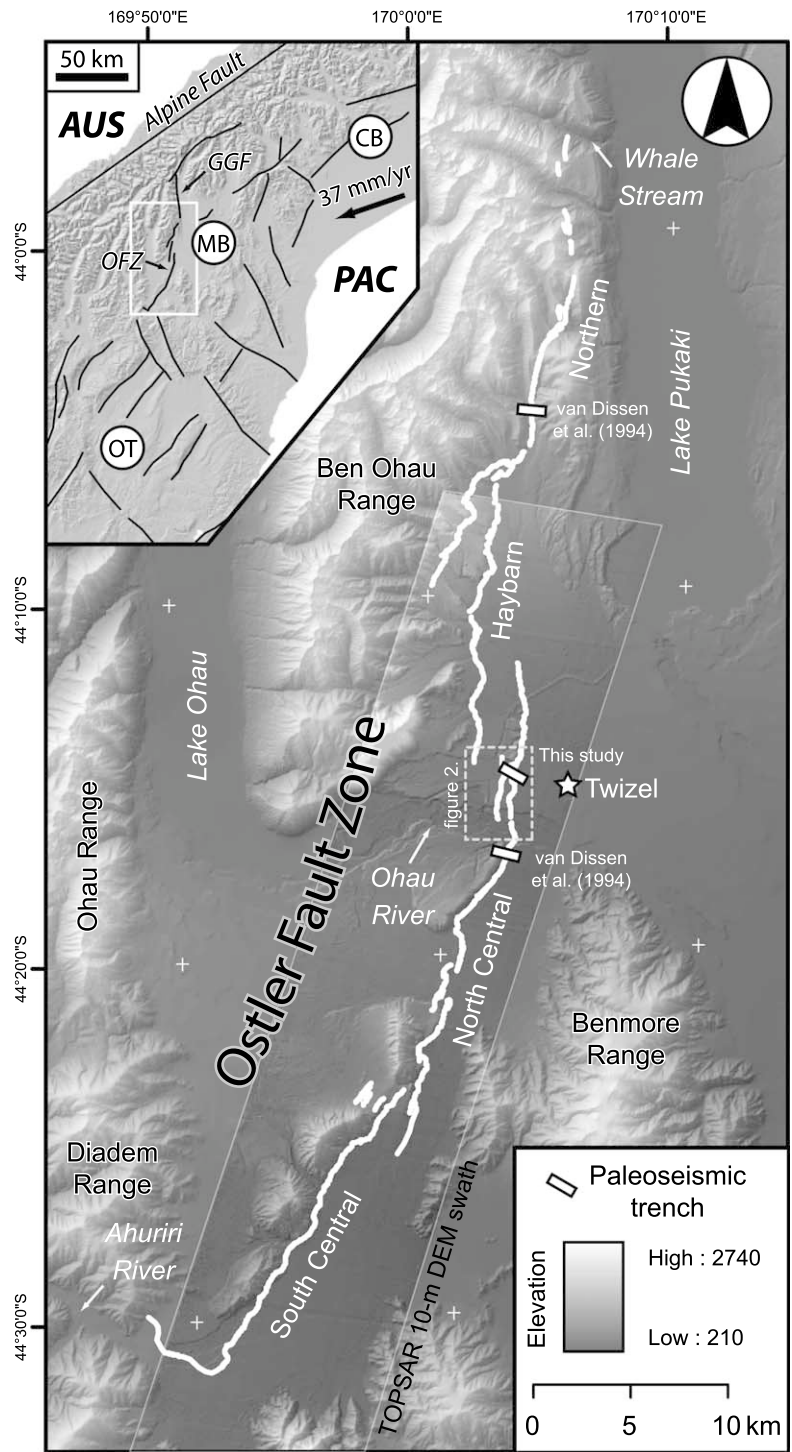


Figure 1 The Ostler fault zone. Overview map shows the location of fault scarps, major fault sections and previous palaeoseismic trenches in the Ohau and Pukaki Valleys. Inset map depicts active fault traces in the Mackenzie Basin (MB), Otago (OT) and Canterbury (CB), as well as the tectonic setting of the obliquely colliding Australian (AUS) and Pacific (PAC) plates. The location of the Ostler fault zone (OFZ) within the small bounding box and the Great Groove fault (GGF) are also shown for reference.

Study area

The Ostler fault spans approximately 60 km in total, from the Ahuriri River in the south to Whale Stream at the northern end of Lake Pukaki (Fig. 1). The fault exhibits an average

strike of 015° (Fig. 1 inset) in a crustal and structural transition zone that interrupts the largely plate-boundary parallel orientation of folds and thrusts in Otago and Canterbury (Upton et al. 2009). Geomorphic offsets along

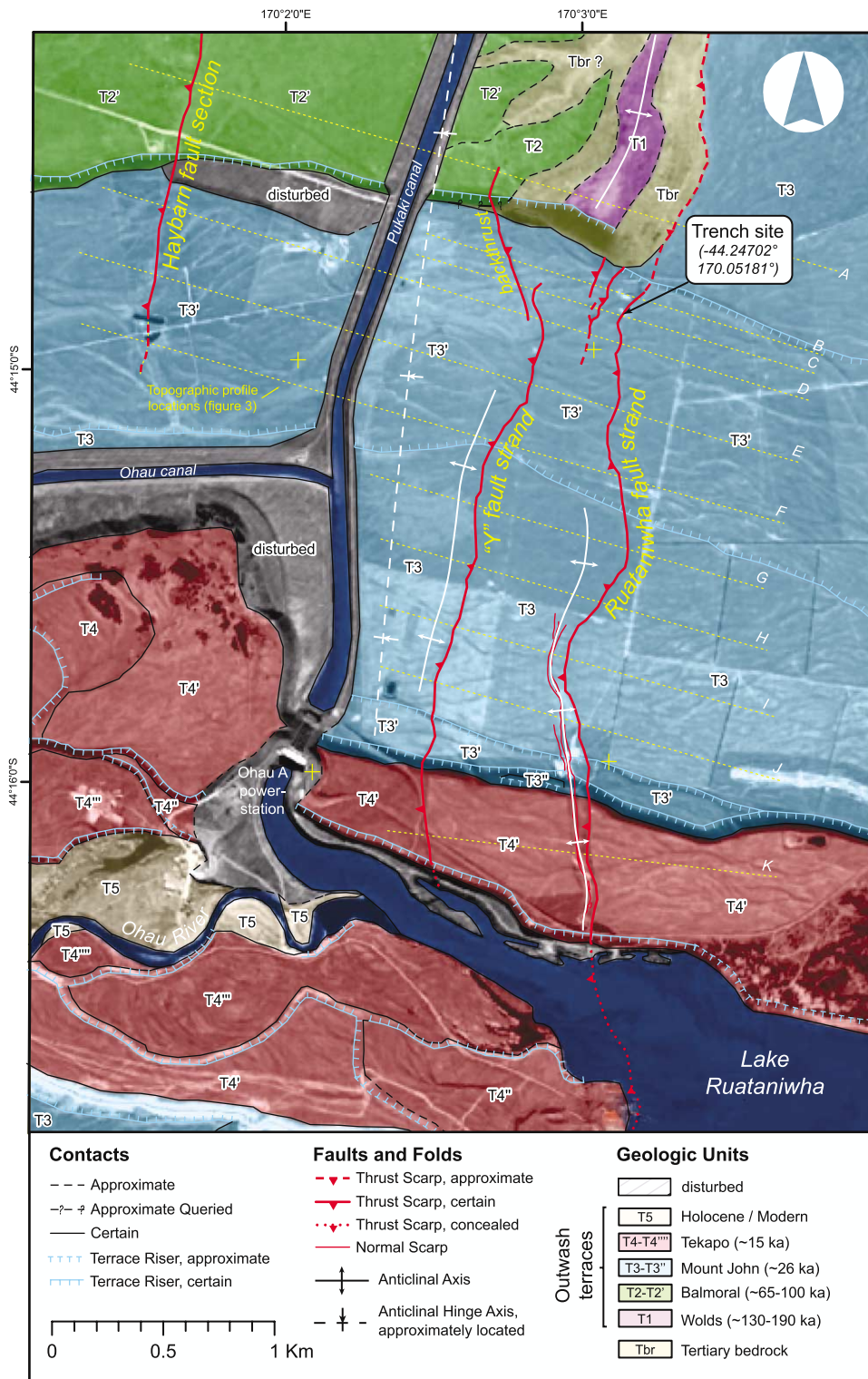


Figure 2 Surficial geologic map of the Ohau River terraces showing the location of fault scarps, fold axes, terrace risers and topographic profiles depicted in Fig. 3.

the fault display primarily west-side-up, reverse displacements without a significant component of strike slip (Read 1984). Seismic reflection profiles across the Ostler fault zone indicate a throw of c. 800 m of Plio-Pleistocene strata

underlying the Mackenzie Basin (Ghissetti et al. 2007). The Ostler fault at its northern end merges with the Great Groove fault, which extends an additional 30 km along the foot of the Ben Ohau Range (Ward & Sporli 1979). With the exception

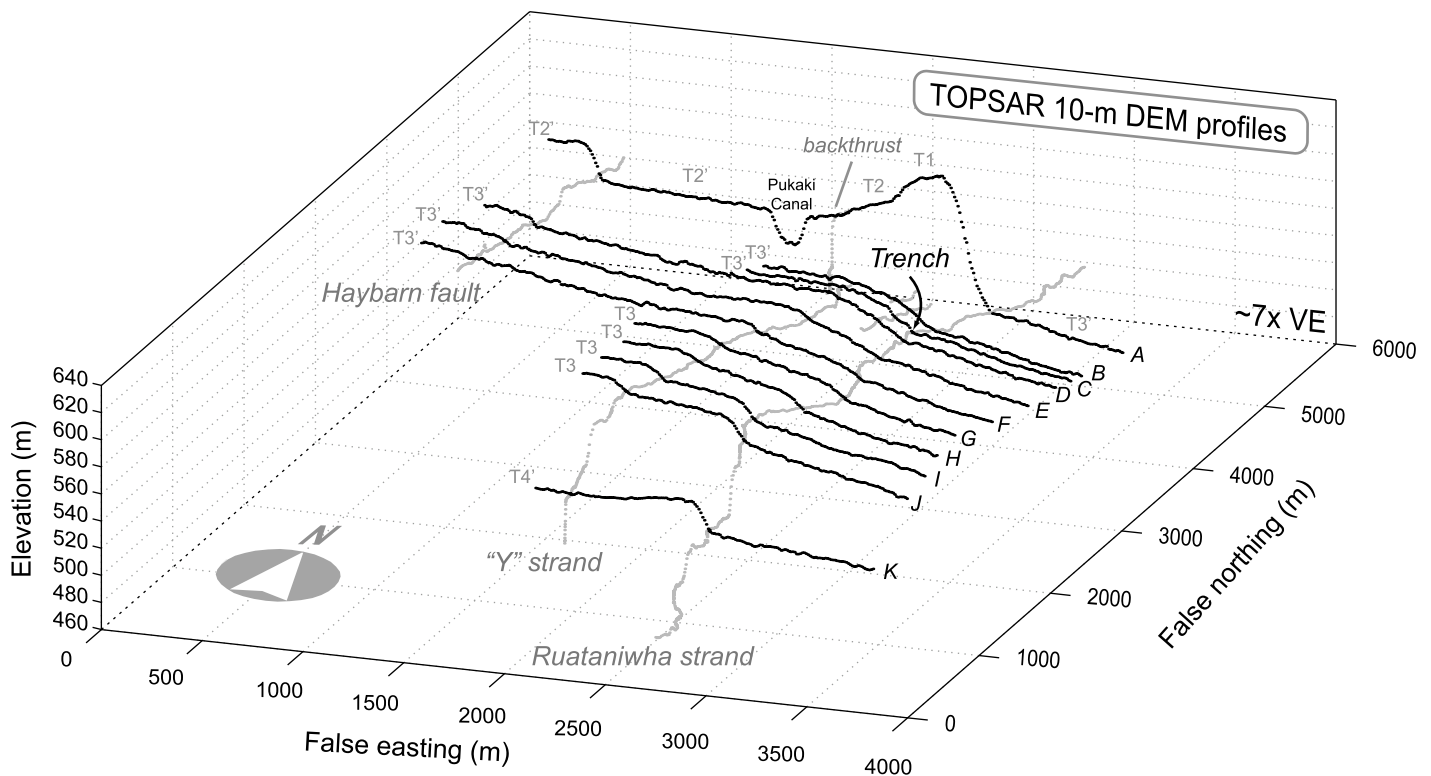


Figure 3 Three-dimensional perspective image of topographic profiles extracted from a TOPSAR 10 m digital elevation model along fault strands (grey) and perpendicular to faults and fold axes (black) on deformed outwash surfaces. Profile locations and corresponding letters are shown in Fig. 2.

of the Great Groove fault, where displacement of Plio-Pleistocene sediments includes both reverse and left-lateral strike-slip components (Templeton et al. 1999), displacement along the Ostler fault zone is considered to be predominately dip slip.

The active surface trace of the Ostler fault is highly segmented and can be subdivided into four primary fault sections and numerous shorter strands based on discontinuities in the surface trace and changes in the overall fault strike (Fig. 1). Complex patterns of surface faulting are common where the fault intersects major transverse drainages or outwash valleys such as the Ohau River (Fig. 2). Despite this surface complexity, the total displacement and fault-slip-rate profile summed for individual strands and across stepovers (Amos et al. 2010) suggests that the entire Ostler fault has behaved as a kinematically linked array (Davis et al. 2005).

Surface deformation patterns across the fault zone are typified by highly asymmetric anticlinal folding with broad west-tilted fold backlimbs abruptly transitioning to relatively steep and short fold forelimbs adjacent to the fault trace (Fig. 3). In an earlier study, we interpreted this pattern as reflecting slip along listric or curvilinear thrusts rooted at shallow depths into planar fault ramps (Amos et al. 2007). Changes in the shape and extent of surface folding (Fig. 3)

reflects substantial along-strike variation in the orientation and geometry of the underlying fault planes potentially controlled in part by changes in the depth and character of underlying Plio-Pleistocene strata. Fault planes imaged using ground-penetrating radar in the shallow subsurface show a range in fault dips of 30–60° (Amos et al. 2007; McClymont et al. 2008; Wallace et al. 2010). This range of fault orientations agrees with geometric estimates made from offsets of multiple terrace levels ($50^\circ \pm 9^\circ$, 1σ ; Davis et al. 2005) and from the range in fault dips imaged using seismic reflection and refraction data (Ghissetti et al. 2007; Campbell et al. 2010).

No major earthquakes have occurred on the Ostler fault since European settlement of the area around 1850. However, previous trenching studies and radiocarbon dating 18 km north of our site (Fig. 1) uncovered colluvial wedge stratigraphy bracketing the timing of two surface-rupturing earthquakes at 2850–4410 cal a BP and 5740–7780 cal a BP, and a third event c. 10 ky ago (van Dissen et al. 1994). In a second trench to the south, these authors also reported a radiocarbon age of 439–674 cal a BP for an unfaulted debris flow overlying the fault immediately south of Lake Ruataniwha and the Ohau River (Fig. 1). We also noted the presence of an approximately 1 m high scarp cutting the foot of young hillslopes outside of transverse drainages along much

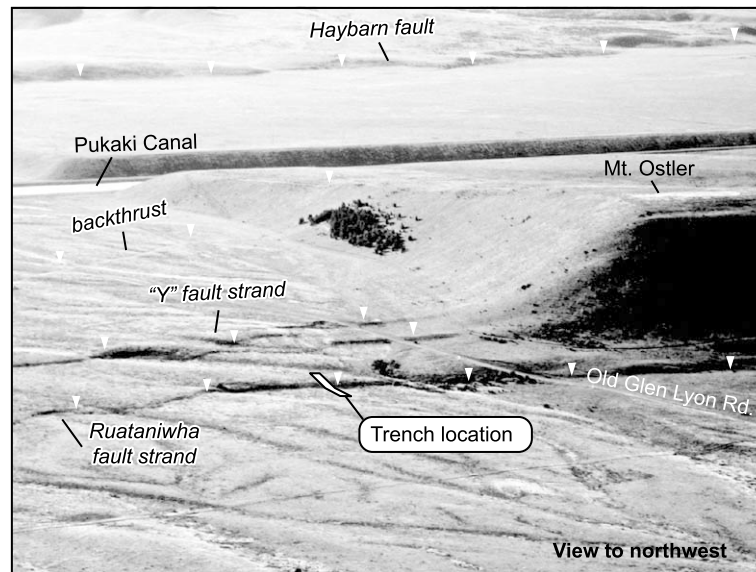


Figure 4 Oblique aerial image of the trench location and other adjacent strands of the North Central and Haybarn fault sections.

of the length of the Ostler fault zone (Amos et al. 2010) that may represent a single-event scarp formed during the most recent earthquake (MRE).

Several generations of Late Pleistocene glacial moraines, outwash surfaces and fluvial terraces generated through repeated glacial occupation of the neighbouring Ohau and Pukaki valleys dominate the surficial geology of the Mackenzie Basin (Read 1984). Four general age divisions of fluvio-glacial landforms and deposits correlate among individual drainages across the fault as originally recognised by Gair (1967). From oldest to youngest, these geomorphic features include the Wolds, Balmoral, Mount John and Tekapo age associations (T1–T4, Fig. 2). A nearly complete sequence of these outwash, strath and cut terrace surfaces is preserved near the trench site flanking the Ohau River and Lake Ruataniwha (Fig. 2). Available cosmogenic radio-nuclide and OSL dating constraints for these landforms indicate stabilisation of the last glacial maximum (LGM) Tekapo T4 and Mount John T3 terrace surfaces at 15.2 ± 2.4 ka and 26.5 ± 4.0 ka, respectively (Schaefer et al. 2001; Amos et al. 2007, 2010). These studies also bracket the formation of the Balmoral T2 and Wolds T1 terraces at approximately 72–105 ka and 130–191 ka respectively, based on OSL dating and correlation with global climate records.

Palaeoseismic trenching

A 26 m long trench was excavated across a 4 m high scarp on the Ruataniwha strand of the Ostler fault (Figs. 3 and 4), located along Old Glen Lyon Rd c. 4 km west of Twizel. This site was chosen based on the location of previous ground-penetrating radar surveys investigating the shallow subsurface structure of the Ostler fault (Nobes et al. 2005). The trench was excavated to an average depth of 2 m into

Mount John outwash gravels and was benched at its lower end to prevent wall collapse. The Ruataniwha strand is one of approximately four scarps within a complex zone of surface faulting (Fig. 4) disrupting the relatively broad LGM outwash plain north of Lake Ruataniwha (Fig. 2). Several minor scarps separate the Ruataniwha strand from the subparallel ‘Y’ fault, which terminates at its northern end into an east-side-up backthrust (Fig. 2). Scarp-perpendicular topographic profiles (Fig. 3) indicate that the trenched fault strand accommodates less than c. 50% of the total displacement of the Mount John surface in this location.

Detailed logging of the exposed stratigraphy was completed at a scale of $1'' = 0.4$ m or c. 1:16 after cleaning the trench walls and stringing with a meter grid. A scaled version of the logged southwestern wall, as well as a composite photomosaic, provides the clearest image of the deformed and faulted stratigraphy (Fig. 5). Collapse of the northern trench wall during excavation immediately adjacent to the exposed fault plane prevented complete logging of this exposure. Nonetheless, a scaled section of the northeastern trench wall (Fig. 6) supplements the analysis of the opposite wall.

The Ruataniwha fault appears within the southwestern trench wall as a gently northwest-dipping discontinuity in otherwise continuous sedimentary layers near the midpoint of the topographic scarp (Fig. 5). This discontinuity defines the main fault plane, which exhibits an average dip of approximately 30° in the upper 2 m of stratigraphy. The fault is not perfectly planar, however, and becomes roughly subhorizontal toward the top of the trench where it nears the ground surface. This transition to an approximately horizontal fault orientation is also observed in the northeastern trench wall (Fig. 6), although the fault plane there reveals a

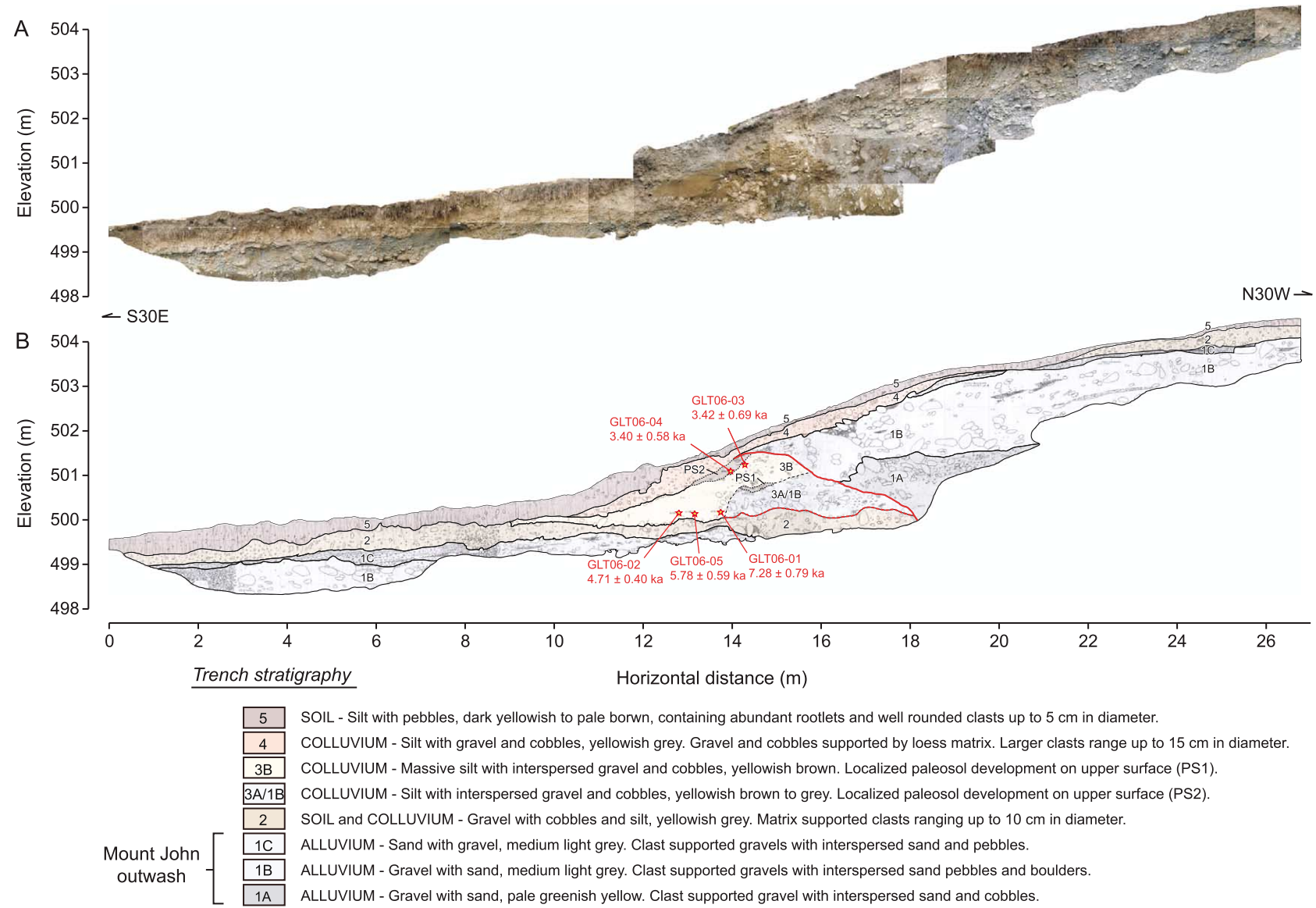


Figure 5 **A**, Photomosaic of the southwestern wall of the Ruataniwha trench exposure. **B**, Annotated trench interpretations overlain on a scaled version of the original trench log. The location of OSL samples and the corresponding sample names are shown by stars. The depositional units (1–4) defined here relate to both trench walls.

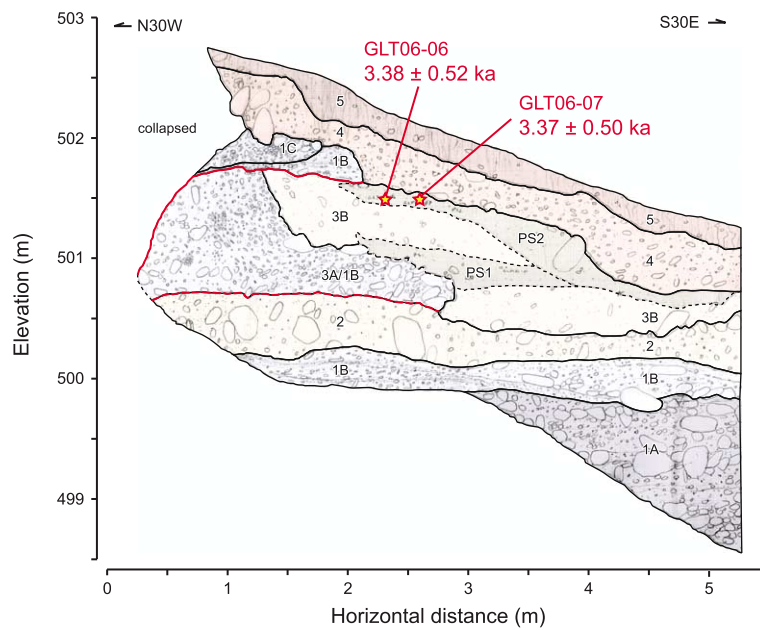


Figure 6 Annotated trench interpretations of the northeastern trench wall are overlain onto a scaled version of the original trench log. The location of OSL samples and the corresponding sample names are shown by stars.

steeper dip of roughly 60° in the lower 2 m. A second subhorizontal strand of the Ruataniwha fault is inferred in each trench wall (dashed red line, Figs. 5 and 6) based on the stratigraphic relationships described below.

We identified eight depositional units (Fig. 5) that enable us to reconstruct the deformational record. In each trench wall (Figs. 5 and 6), we encountered relatively loose and sandy gravels beneath the overlying soil as well as several packages of mixed silt and gravel immediately underlying the topographic scarp. The lowest stratigraphic units exposed in each trench comprise intact open-framework alluvial gravels with interspersed boulders and sand lenses towards the top of the deposit (Units 1A-C, Figs. 5 and 6). We interpret these units as the original Mount John outwash gravels deposited during formation of the T3' braid plain (Fig. 2). The lowest member of Unit 1 is only exposed on the upthrown western side of the fault plane. Directly overlying

Unit 1 is a package of soil and colluvium, derived from and developed directly on the lower alluvial gravels (Unit 2, Figs 5 and 6). The matrix-supported nature of this deposit and its pale yellow-to-brown colour serve to distinguish Unit 2 from the grey imbricated gravels of the underlying outwash (Fig. 5). In both trench walls, Unit 2 is observed in conformable contact above Unit 1 on the downthrown southeastern side of the main fault plane (Figs. 5 and 6).

A succession of yellowish-brown massive silt with interspersed cobbles and gravel (Units 3A and B) unconformably overlies Unit 2 and rests in fault contact with intact outwash gravels on the upthrown northwestern side of the fault (Fig. 5). The rubbly nature of this matrix-supported deposit suggests its origin as colluvium derived from the Ruataniwha scarp. Unit 3 is divided into two sub-units (3A and 3B) based on the relative abundance of coarser material. In addition to silt, the lower Unit 3A contains abundant

Table 1 Luminescence dating results: water and radionuclide contents.

Sample number	Depth (m)	Water content δ^1	U ($\mu\text{g/g}$) from ^{234}Th	U ($\mu\text{g/g}$) ² from ^{226}Ra , ^{214}Pb , ^{214}Bi	U ($\mu\text{g/g}$) from ^{210}Pb	Th ($\mu\text{g/g}$) ² from ^{208}Tl , ^{212}Pb , ^{228}Ac	K (%)	Field Code
WLL570	1.39	1.264	3.28 ± 0.31	3.13 ± 0.21	2.51 ± 0.27	10.91 ± 0.15	1.54 ± 0.04	GLT06-01
WLL571	1.15	1.218	3.37 ± 0.32	3.22 ± 0.21	2.94 ± 0.28	10.53 ± 0.15	1.57 ± 0.04	GLT06-02
WLL572	0.60	1.211	3.58 ± 0.24	3.24 ± 0.16	3.26 ± 0.21	11.06 ± 0.13	1.53 ± 0.03	GLT06-03
WLL573	0.60	1.279	3.42 ± 0.35	3.16 ± 0.23	2.80 ± 0.30	11.33 ± 0.17	1.50 ± 0.04	GLT06-04
WLL574	1.28	1.241	3.31 ± 0.32	2.68 ± 0.20	2.64 ± 0.26	10.44 ± 0.15	1.55 ± 0.04	GLT06-05
WLL575	0.73	1.229	3.50 ± 0.31	2.96 ± 0.20	3.07 ± 0.27	11.29 ± 0.15	1.59 ± 0.04	GLT06-06
WLL576	0.61	1.236	3.17 ± 0.33	3.12 ± 0.22	2.87 ± 0.29	11.08 ± 0.16	1.55 ± 0.04	GLT06-07

¹Ratio wet sample to dry sample weight. Errors assumed 50% ($\delta-1$)

²U and Th-content is calculated from the error-weighted mean of the isotope equivalent contents. Italics indicate a radioactive disequilibrium on a 2 σ level.

cobbles, gravel and pebbles that were apparently derived from the adjacent Unit 1B, implying that Unit 3A originated as either colluvium shed from this older unit or as a piece of relatively intact stratigraphy thrust over a subhorizontal fault surface overlying Unit 2 (dashed red line, Figs. 5 and 6). Although Units 1B and 3A differ in colour across the fault, steeply southeast-dipping clasts observed within Unit 3A on the northeastern trench wall (Fig. 6) may imply rotation of original Unit 1B outwash stratigraphy over the former ground surface during a faulting event. The relative abundance of massive silt within the overlying Unit 3B suggests a partially aeolian origin, possibly as wind-blown loess trapped against the lee side of the topographic scarp. Aeolian input into unit 3B may also explain its relative thickness in comparison with younger colluvial units (Fig. 5). Two darker-brown concentrations of silt with lesser pebbles at the top and base of Unit 3B are interpreted as palaeosols (Units PS1 and PS2, Figs. 5 and 6) buried by and formed on scarp-derived colluvium and loess.

The uppermost stratigraphic units overlie all strands of the Ruataniwha fault (Figs. 5 and 6). The older of these two deposits (Unit 4) consists of silt with interspersed gravel and cobbles. The rubbly matrix-supported character of this unit, in addition to its topographic position along the scarp, suggests an origin as scarp-derived colluvium shed from the scarp face (Figs. 5 and 6). Lastly, the ground surface is immediately underlain by c. 20–40 cm of modern topsoil, Unit 5, which represents an organic-rich A-horizon developed on the underlying colluvium.

OSL dating

A total of seven OSL samples (Tables 1 and 2 and Fig. 7) were collected from silt contained within the colluvial wedge of Unit 3B and the overlying palaeosol PS2 (Figs. 5 and 6). The validity of these OSL ages depends upon sufficient exposure to sunlight prior to burial so that each sample is effectively reset to zero (Duller et al. 1996; Aitken, 1998). Although questions surround the suitability of coarse colluvium shed during scarp retreat events, OSL dating has proven effective in palaeoseismic efforts to date finer-grained scarp colluvium or buried soil horizons (Forman et al. 2000). As such, we sampled the silty portions of buried soil and colluvial deposits, which represent reworked loess that originally accumulated along the topographic scarp.

All samples were prepared and analysed at the Luminescence Dating Laboratory, School of Earth Sciences, Victoria University, Wellington, NZ. The palaeodose, i.e. the radiation dose accumulated in each sample after the last light exposure, was determined by measuring the blue luminescence output during infrared optical stimulation, which selectively stimulates the feldspar fraction. Palaeodoses were estimated using the multiple aliquot-dose method with late light subtraction. A 'plateau test' was completed for each sample by comparing early and later portions of the

resulting shinedown curve as a test for partial resetting of the OSL age. The dose rate was estimated based on low-level gamma spectrometry measurements.

The probability distributions of three samples from palaeosol Unit PS2 and one from colluvial Unit 3B yield a remarkably tight cluster of ages centred at 3.4 ± 1.1 ka (2σ) (Fig. 7). The approximately normal distribution of these ages suggests that the associated errors reflect uncertainties in the analytical measurement only. Several possible depositional histories explain the similarity in ages from both buried soil and colluvial units. First, these samples may have undergone complete resetting of their OSL ages during soil formation, which presumably involved reworking of finer-grained loess present along the former scarp. Alternatively, the ages of these samples may reflect their depositional origin as loess, which ceased to accumulate during scarp retreat after a faulting event. The presence of soil at the top of colluvial Unit 3B, however, implies some residence time for this material along the former scarp face. We therefore favour the former scenario where the OSL ages reflect the timing of tectonic burial during surface faulting and subsequent scarp retreat. In either case, these dates together provide a minimum age for Unit 3B of 2.3–4.5 ka.

Three samples collected near the base of colluvial Unit 3B provide a larger spread in age, ranging 4.1–8.4 ka at 95% confidence (Fig. 7). Despite this spread, we note a progression in age from oldest to youngest away from the toe of colluvial Unit 3A. This age sequence may reflect progressive reworking of loess as finer-grained colluvium at the base of the former fault scarp. Alternatively, this progression of ages could be explained by partial resetting of silt grains during deposition of the colluvial wedge, although the plateau test for these samples shows no indication of incomplete resetting of the OSL age. In either scenario, this range places a maximum bound on the age of colluvial Unit 3B (Fig. 5).

Characterisation of past earthquakes

Scarp-derived colluvial wedges within the exposed trench stratigraphy inform the history of past surface-rupturing earthquakes along the Ruataniwha fault. These deposits imply a relatively sudden over-steepening of the scarp face during an earthquake event, followed by erosion of the top of the scarp and deposition at its base. Scarp retreat represents a punctuated event in time and is considered diagnostic of coseismic displacement at the trench scale (e.g., McCalpin et al. 2009). In contrast, steadier fault creep at the ground surface would result in gradual deposition of finer colluvium at the base of the scarp that thickens away from the fault zone (Lienkaemper et al. 2002), akin to growth strata deposited along the flanks of an actively growing fold. We therefore consider the rubbly colluvial deposits encountered in our trench as direct evidence for scarp retreat driven

Table 2 Luminescence dating results: measured a -value and equivalent dose, cosmic doserate, total doserate and OSL age.

Sample number	a -value	D_e (Gy)	dD_e/dt (Gy/ka) ¹	dD/dt (Gy/ka)	OSL-age (ka)	Field code
WLL570	0.086 ± 0.013	26.1 ± 1.9	0.1834 ± 0.0092	3.59 ± 0.29	7.28 ± 0.79	GLT06-01
WLL571	0.073 ± 0.015	17.1 ± 0.6	0.1896 ± 0.0095	3.63 ± 0.28	4.71 ± 0.40	GLT06-02
WLL572	0.072 ± 0.019	12.6 ± 2.3	0.2046 ± 0.0102	3.68 ± 0.30	3.42 ± 0.69	GLT06-03
WLL573	0.066 ± 0.013	11.5 ± 1.7	0.2046 ± 0.0102	3.38 ± 0.29	3.40 ± 0.58	GLT06-04
WLL574	0.072 ± 0.013	19.3 ± 1.3	0.1862 ± 0.0093	3.34 ± 0.26	5.78 ± 0.59	GLT06-05
WLL575	0.082 ± 0.019	12.5 ± 1.6	0.2009 ± 0.0100	3.70 ± 0.31	3.38 ± 0.52	GLT06-06
WLL576	0.082 ± 0.013	12.4 ± 1.6	0.2043 ± 0.0102	3.68 ± 0.28	3.37 ± 0.50	GLT06-07

¹Contribution of cosmic radiation to the total doserate, calculated as proposed by Prescott & Hutton (1995).

by past surface-rupturing earthquakes. In this interpretation, the base of each colluvial deposit represents an event horizon bracketing the timing of earthquake displacement.

Within the Ruataniwha trench, colluvial debris truncates the exposed fault plane as well as older, underlying colluvial units, implying deposition of Unit 4 during erosional stripping of the scarp face after the most recent earthquake (Figs. 5 and 6). Accordingly, topsoil developed on this unit thickens at the foot of the scarp and thins towards the top (Fig. 5). Although a paucity of readily datable material prevents a precise age estimate of Unit 4, OSL ages on the underlying colluvial wedge (Units 3A and B) provide a maximum bound on the MRE. A composite age from four OSL samples within these units brackets the timing of the MRE to some time after 2.3–4.5 ka (95% confidence) (Fig. 7). Slip during this event along the main fault plane resulted in offset of the contact between Units 3A and B, totalling at least 1.8 m (Fig. 5). This measurement represents a minimum estimate on the total displacement during the MRE given that the Unit 3A/3B contact was eroded on the upthrown northwestern side of the fault.

Faulted colluvial deposits of Units 3A and B also imply the presence of an earlier earthquake. OSL dates from silt collected at the base of Unit 3B provide a minimum age of

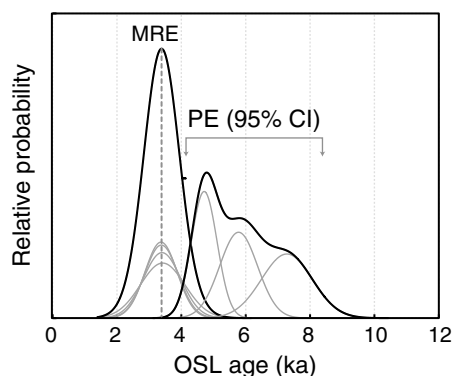


Figure 7 Probability density functions for all reported OSL ages and the associated standard errors. Composite probability functions for the most recent earthquake (MRE) and the penultimate event (PE) are shown in black. The vertical dashed line indicates a composite age peak of 3.4 ± 1.1 ka for the MRE. 95% confidence intervals (CI) bracket the timing of the PE to before 4.1–8.4 ka.

4.1–8.4 ka (95% confidence) on the timing of the penultimate event (Fig. 7). Constraints on the total displacement during this event are less well bracketed than for the MRE. If Unit 3A represents a relatively intact section of Unit 1B outwash gravels overthrust subhorizontally onto Unit 2, then the total offset during this event exceeded 2.5 m (Fig. 6) and may have been as large as 4 m (Fig. 5). Given that no equivalent unit exists on the upthrown side of the fault, an alternative interpretation of Unit 3A as a colluvium derived from Units 1 and 2 would indicate a comparable or larger surface displacement. However, the presence of apparently rotated imbricate clasts in the northeastern trench wall (Fig. 6) favours the former scenario and implies that these gravels were essentially ‘bulldozed’ onto the old ground surface during the penultimate earthquake. This contact now defines an approximately flat or undulatory fault surface in the exposed trench stratigraphy. The subhorizontal nature of this structure reflects the former ground surface rather than the fault plane orientation in the deeper subsurface.

Continuity in the outwash stratigraphy on either side of the southwestern trench wall provides constraints on the total offset of the Mount John outwash. Offset of sand lenses at the top of Unit 1 (Unit 1C, Fig. 5) imply c. 2.9 m of throw across the fault, corresponding to a dip slip of c. 6.0 m over a 30° fault plane. Given our constraints on the coseismic slip during the MRE and penultimate events, this magnitude of displacement implies a maximum of only 2–3 events on the trenched fault strand since deposition of the LGM outwash surface.

Discussion

Coarse colluvial wedge deposits abutting and overlying the Ruataniwha fault strand provide stratigraphic evidence of past, coseismic surface ruptures along the central Ostler fault zone (Figs. 5 and 6). Again, these deposits originate from oversteepening of the scarp face during earthquake events and are considered unique to coseismic deformation as opposed to ongoing fault creep. Our results corroborate previous trenching studies on the Northern Ostler fault (van Dissen et al. 1994) that demonstrate similar palaeoseismic evidence for ancient coseismic displacements, despite on-

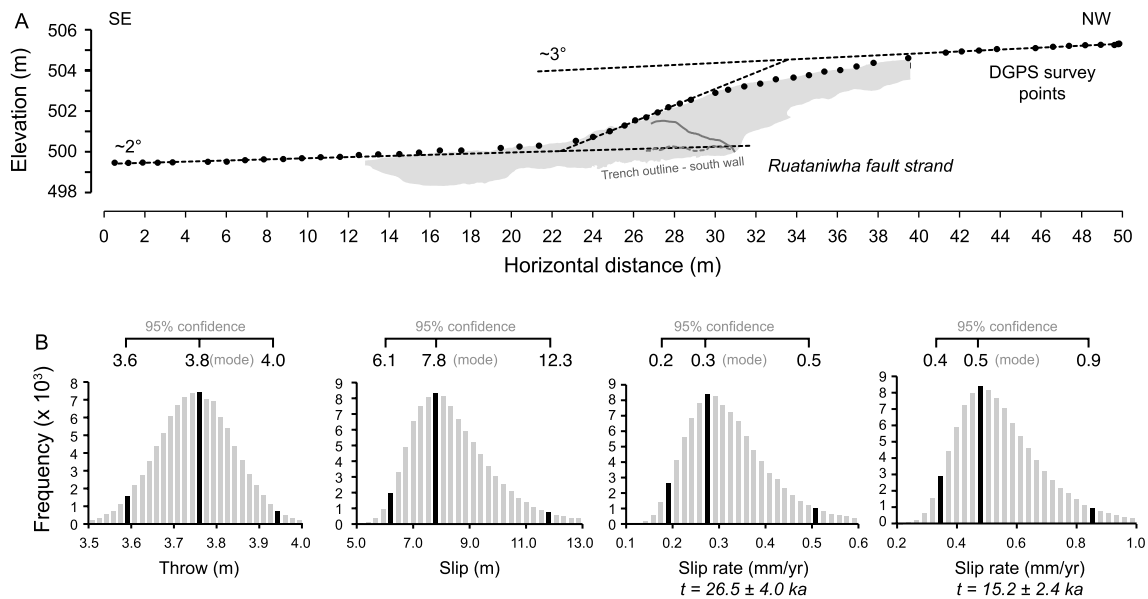


Figure 8 **A**, Scarp-perpendicular profile points across the Ruataniwha fault from differential GPS surveying are overlain on an outline of the southwestern trench wall. Linear regressions through intact portions of the footwall, hanging wall and scarp face are used to calculate histograms of throw, fault slip and dip-slip rate shown in **B**. Reported values for each parameter reflect the histogram mode and the associated 95% confidence intervals.

going aseismic deformation localised near our trench site. Geodetic monitoring of a levelling route passing within metres of our trench along Glen Lyon Road indicated relatively continuous growth of a hanging wall anticline with a maximum uplift rate of c. 1 mm a^{-1} over the period 1966–1989 (Blick et al. 1989). Folding over this time interval mimics the overall shape and wavelength of the warped LGM outwash surface, but occurred without a net vertical displacement over the fault zone. As such, Blick et al. (1989) attributed the permanent vertical component of the total deformation observed in 10^4 – 10^5 year old geomorphic offsets to coseismic slip. Our results confirm that a significant component of the total vertical offset of outwash stratigraphy occurs during past surface-rupturing earthquakes.

Folding at the trench scale also accommodates some component of the total deformation across the Ruataniwha fault. Comparison of fault offset observed in the trench exposures with that implied by the height of the topographic scarp constrains the relative contribution of surface folding to the total deformation. Survey profiling at the trench site using a differential GPS indicates a throw of $3.8 \pm 0.2 \text{ m}$, corresponding to an offset of $7.8 + 4.5 / -1.7 \text{ m}$ at 95% confidence (Fig. 8). Assuming purely dip slip, this calculation utilises a fault dip of $30^\circ \pm 10^\circ$ (2σ) and standard errors on linear survey regressions, following the Monte Carlo approach developed by Thompson et al. (2002). Using age estimates bracketing the timing of LGM outwash deposition, this offset corresponds to a range in dip-slip rates between 0.3 and 0.5 mm a^{-1} (Fig. 8). The throw of Unit 1C measured from the southwestern trench exposure (Fig. 5) totals 2.9 m and indicates total offset of the Mount John

outwash of the order c. 6 m . This measurement fails to capture the total deformation of this deposit, however, by neglecting additional folding of the hanging-wall surface immediately adjacent to the Ruataniwha fault (Fig. 8). Results from our surveyed profiles indicate that surface folding accounts for roughly 25% of the total 7.8 m dip-slip accommodated across the scarp.

It remains unknown whether folding at the trench scale reflects permanent deformation related to aseismic fault slip. Alternatively, localised folding adjacent to the Ruataniwha fault may be driven by relatively shallow gradients in fault slip during earthquake surface ruptures. Given that approximately 75% of the total offset across the Ruataniwha scarp is linked to coseismic fault slip, the majority of strain on this fault strand appears to be released during seismic events. Despite folding observed from levelling measurements over the past several decades (Blick et al. 1989), our trenching results suggest that aseismic deformation, if retained as permanent deformation, is outpaced by coseismic slip integrated over longer time intervals.

Coseismic slip during the MRE resulted in at least 1.8 m of offset of the Unit 3A/1B contact (Fig. 5). Treating this value as a minimum constraint on the total coseismic slip suggests a possible range of earthquake magnitudes up to **M** 6.9–7.1 using the empirical relationships of Wells & Copper-smith (1994). Similarly, these relationships indicate possible earthquake magnitudes up to **M** 7.1 if the entire c. 60 km surface trace of the Ostler fault zone (Fig. 1) were to rupture in a single event.

Similarity in the timing of both the MRE and penultimate earthquake on the North Central Ostler fault ($< 3.4 \pm 1.1 \text{ ka}$

and > 4.1–8.4 ka, respectively) with reported radiocarbon age estimates of these events 18 km to the north (2850–4410 cal a BP and 5740–7780 cal a BP; van Dissen et al. 1994) suggests the possibility of synchronous fault rupture between these fault sections. Together with the radiocarbon age on an unfaulted debris flow south of Lake Ruataniwha, our study indicate that the MRE on the North Central Ostler fault occurred between 439–674 cal a BP (van Dissen et al. 1994) and 2.3–4.5 ka. These ages indicate that the MRE observed in our trench may have been part of a larger fault rupture affecting northern sections of the fault. If indeed true, stepovers between these fault sections up to 2.5 km wide (Figs. 1 and 2) did not serve as barriers to rupture propagation. Available compilations for strike-slip faults suggest that this value lies below the limiting dimension of fault stepovers as endpoints to earthquake ruptures (Wesnousky 2006). This result carries implications for seismic hazard assessments in the area, which must therefore include the possibility of total fault rupture of the entire c. 60 km long Ostler fault zone.

Despite the possibility of total fault rupture during large earthquakes, the presence of only 2–3 surface ruptures on the Ruataniwha fault in the last 26.5 ka raises the possibility that nearby strands (Fig. 2) may accommodate other events not recorded along this scarp. The timing of Holocene events on the trenched Ruataniwha fault and those uncovered in previous trench investigations (van Dissen et al. 1994) suggests an average earthquake recurrence interval of roughly 2–5 ka, albeit spanning only 2–3 events. Given the age of the Mount John surface, a constant recurrence interval would suggest an additional 2–10 fault ruptures since deposition on this surface ceased. These earthquakes need not recur at a constant interval, however, as evidenced by similar total deformation of the Mount John and Tekapo outwash surfaces near Lake Ruataniwha (compare profiles I and K on Fig. 3) despite a c. 10 ka difference in age. Comparable offsets of each of these two surfaces may also reflect along-strike changes in both the shape and amplitude of the scarp or the hanging-wall anticline (Fig. 3) as slip is transferred among individual fault strands (Davis et al. 2005).

Clearly, the Ruataniwha fault represents only one of several additional strands within this part of the North Central Ostler fault that accommodate additional slip and/or drive folding of the ground surface (Figs. 2 and 3). Total offset across both the Ruataniwha and Y fault strands of North Central fault section, calculated from topographic profiles on the Mount John surface, totals approximately 29 m (Amos et al. 2010). Of the c. 20 m of dip slip on the Ruataniwha fault, only c. 8 m of total offset occurs along the trenched strand. As such, an additional c. 12 m of slip must occur on other adjacent fault segments or be accommodated by hanging-wall folding (Fig. 3). This result emphasises the importance of tradeoffs in displacement among overlapping fault strands within a kinematically linked fault array.

Summary

The results of trench analysis and OSL dating along the Ruataniwha strand of the Ostler fault zone allow us to make the following conclusions.

1. Palaeoseismic trenching reveals evidence for at least two metre-scale coseismic surface displacements along the North Central Ostler fault zone. Despite geodetically observed aseismic deformation in this location that approaches the total vertical slip rate on the fault, most strain on the Ostler fault zone is released during large surface-rupturing earthquakes.
2. Interpretation of colluvial wedge stratigraphy and optically stimulated luminescence dating in trench exposures defines the most recent surface rupture on the Ostler fault as younger than 2.3–4.5 ka, whereas the penultimate event pre-dates 4.1–8.4 ka.
3. Surface offset during the most recent earthquake exceeded 1.8 m. Using the c. 60 km total length of the Ostler fault zone, this value of coseismic slip is consistent with earthquake magnitudes ranging up to M 6.9–7.1. Surface displacement during the penultimate event is not as well constrained, but likely exceeded the total slip during the most recent earthquake.
4. Folding at the trench scale accounts for roughly 25% of the total offset measured from topographic profiling of the deformed ground surface (7.8 m) when compared with offset of Mount John outwash gravels (6.0 m) observed in trench exposures. This folding may reflect either retention of aseismic slip, i.e. fault creep, as a component of the permanent deformation or shallow subsurface gradients in fault slip during coseismic displacement.
5. Similarity between the timing of past earthquakes on the central and northern Ostler fault zone suggests that surface ruptures may persist across major fault-section boundaries delineated by kilometre-scale stepovers and changes in strike of the active surface trace.
6. If large surface ruptures on the Ostler fault recur every c. 2–5 ka, evidence for only 2–3 palaeoearthquakes affecting the 26.5 ka Mount John outwash surface trenched in this study indicates that additional events likely occurred on adjacent scarps within an overall complex zone of surface faulting.

Acknowledgements

We thank the Hocken family for permission to access and excavate a fault trench on their land. Jocelyn Campbell, Art Bettis and Haikai Tane graciously provided trench review. We also thank Mrs Ningsheng Wang at the Luminescence Dating Facility, Victoria University of Wellington, for preparing the OSL samples. Helpful reviews by Tim Little and Francesca Ghisetti improved the quality and clarity of the manuscript. This research was supported by National Science Foundation grant EAR-0117242 and ACS

Petroleum Research Fund grant 41960-AC8. Support for J. Lapwood came from the Mason Trust at the University of Canterbury. We also thank NASA for providing the TOPSAR digital elevation model of the study area.

References

- Aitken MJ 1998. An introduction to optical dating; the dating of Quaternary sediments by the use of photon-stimulated luminescence, Oxford University Press, Oxford, United Kingdom (GBR). 267 p.
- Amos CB, Burbank DW, Nobes DC, Read SAL 2007. Geomorphic constraints on listric thrust faulting: Implications for active deformation in the Mackenzie Basin, South Island, New Zealand. *Journal of Geophysical Research-Solid Earth* 112: B03S11, doi:10.1029/2006JB004291.
- Amos CB, Burbank DW, Read SAL 2010. Along-strike growth of the Ostler fault, New Zealand: Consequences for drainage deflection above active thrusts. *Tectonics* 29(4): TC4021, 10.1029/2009TC002613.
- Blick GH, Read SAL, Hall PT 1989. Deformation monitoring of the Ostler fault zone, South Island, New Zealand. *Tectonophysics* 167: 329–339, doi:10.1016/0040-1951(89)90083-8.
- Campbell FM, Ghisetti F, Kaiser AE, Green AG, Horstmeyer H, Gorman AR 2010. Structure and evolution of the seismically active Ostler Fault Zone (New Zealand) based on interpretations of multiple high resolution seismic reflection profiles. *Tectonophysics* 495(3–4): 195–212.
- Davis K, Burbank DW, Fisher D, Wallace S, Nobes D 2005. Thrust-fault growth and segment linkage in the active Ostler fault zone, New Zealand. *Journal of Structural Geology* 27(8): 1528–1546, doi:10.1016/j.jsg.2005.04.011.
- DeMets C, Gordon RG, Argus DF, Stein S 1994. Effect of recent revisions to the geomagnetic reversal time-scale on estimates of current plate motions. *Geophysical Research Letters* 21(20): 2191–2194, doi:10.1029/1999GL900405.
- Duller GAT 1996. Recent developments in luminescence dating of Quaternary sediments. *Progress in Physical Geography* 20(2): 127–145.
- Forman SL, Pierson J, Letter K 2000. Luminescence Geochronology. In: Sowers JM, Noller JS, Lettis WR ed. *Quaternary Geochronology: Methods and Applications*, American Geophysical Union Reference Shelf 4: 157–176.
- Gair HS 1967. Sheet 20-Mt. Cook. Geological Map of New Zealand [Geological Map of New Zealand]. Wellington, NZ, Department of Scientific and Industrial Research.
- Ghisetti FC, Gorman AR, Sibson RH 2007. Surface breakthrough of a basement fault by repeated seismic slip episodes: The Ostler Fault, South Island, New Zealand. *Tectonics* 26: TC6004, doi:10.1029/2007TC002146.
- Lienkaemper JJ, Dawson TE, Personius SF, Seitz GG, Reidy LM, Schwartz DP 2002. A record of large earthquakes on the southern Hayward fault for the past 500 years. *Bulletin of the Seismological Society of America* 92(7): 2637–2658.
- McCalpin JP, Rockwell TK, Weldon Ii RJ 2009. Chapter 6 Paleoseismology of Strike-Slip Tectonic Environments. In: James PM ed. *Paleoseismology*, International Geophysics Series Vol. 95, Academic Press. Pp. 421–496.
- McClymont AF, Green AG, Villamor P, Horstmeyer H, Grass C, Nobes DC 2008. Characterization of the shallow structures of active fault zones using 3-D ground-penetrating radar data. *Journal of Geophysical Research-Solid Earth* 113(B10).
- Nobes D, Burbank D, Amos C, Davis K 2005. 3D Imaging of the fore- and backthrusts of the Glen Lyon segment of the Ostler Fault. In: Pettinga JR, Wandres AM ed. *50th Annual Conference*. Pp. 61.
- Norris RJ, Cooper AF 2001. Late Quaternary slip rates and slip partitioning on the Alpine Fault, New Zealand. *Journal of Structural Geology* 23(2–3): 507–520, doi:10.1016/S0191-8141(00)00122-X.
- Pearson CF, Beavan J, Darby DJ, Blick GH, Walcott RI 1995. Strain Distribution across the Australian Pacific Plate Boundary in the Central South-Island, New-Zealand, from 1992 Gps and Earlier Terrestrial Observations. *Journal of Geophysical Research-Solid Earth* 100(B11): 22071–22081, doi:10.1029/95JB02279.
- Prescott JR, Hutton JT 1995. Environmental Dose-Rates and Radioactive Disequilibrium from Some Australian Luminescence Dating Sites. *Quaternary Science Reviews* 14(4): 439–448.
- Read SAL 1984. The Ostler Fault Zone. In: Wood PR ed. *Guidebook to the South Island Scientific Excursions International Symposium on Recent Crustal Movements of the Pacific Region*. Wellington, NZ, The Royal Society of New Zealand. Pp. 121–134.
- Read SAL, Blick GH 1991. Late Quaternary deformation and geodetic monitoring in the area of “the knot” on the Ostler fault zone, South Island, New Zealand. *New Zealand Geological Survey Record* 43: 85–91.
- Schaefer JM, Ninnemann U, Denton GH, Schluechter C, Ivy-Ochs S, Wieler R, Kubik PW, Anderson BG, Schlosser P 2001. Structure of the Last Glacial Maximum in New Zealand - Terrestrial and Marine Evidence from Southern mid-latitudes. *American Geophysical Union fall meeting* 82(47): Fall Meet. Suppl., Abstract PP42B-0499.
- Templeton AS, Craw D, Koons PO, Chamberlain CP 1999. Near-surface expression of a young mesothermal gold mineralizing system, Sealy range, Southern Alps, New Zealand. *Mineralium Deposita* 34(2): 163–172.
- Thompson SC, Weldon RJ, Rubin CM, Abdrakhmatov K, Molnar P, Berger GW 2002. Late Quaternary slip rates across the central Tien Shan, Kyrgyzstan, Central Asia. *Journal of Geophysical Research, B, Solid Earth and Planets* 107 (B9), 2203, doi:10.1029/2001JB000596.
- Upton P, Koons PO, Craw D, Henderson CM, Enlow R 2009. Along-strike differences in the Southern Alps of New Zealand: Consequences of inherited variation in rheology. *Tectonics* 28: Tc2007, 10.1029/2008TC002353.
- van Dissen RJ, Hull AG, Read SAL 1994. Timing of some large Holocene earthquakes on the Ostler Fault, New Zealand. *Proceedings of the CRCM 1993*: 381–386.
- Wallace SC, Nobes DC, Davis KJ, Burbank DW, White A 2010. Three-dimensional GPR imaging of the Benmore anticline and step-over of the Ostler Fault, South Island, New Zealand. *Geophysical Journal International* 180(2): 465–474.
- Ward CM, Sporli KB 1979. Exceptionally large steeply plunging folds in the Torlesse Terrace, New Zealand. *Journal of Geology* 87: 187–193.
- Wells DL, Coppersmith KJ 1994. New empirical relationships among magnitude, rupture length, rupture width, rupture area, and surface displacement. *Bulletin of the Seismological Society of America* 84: 974–1002.
- Wesnousky SG 2006. Predicting the endpoints of earthquake ruptures. *Nature* 444(7117): 358–360.